ACS APPLIED MATERIALS & INTERFACES

Research Article

www.acsami.org

Chemical Warfare Agents Detoxification Properties of Zirconium Metal–Organic Frameworks by Synergistic Incorporation of Nucleophilic and Basic Sites

Rodrigo Gil-San-Millan,[†] Elena López-Maya,[†] Morgan Hall,[‡] Natalia M. Padial,[§] Gregory W. Peterson,[‡] Jared B. DeCoste,[‡] L. Marleny Rodríguez-Albelo,[†] J. Enrique Oltra,[§] Elisa Barea,[†] and Jorge A. R. Navarro*[,†]

[†]Departamento de Química Inorgánica, Universidad de Granada, Avenida Fuentenueva S/N, 18071 Granada, Spain

[‡]Edgewood Chemical Biological Center, Aberdeen Proving Ground, Maryland 21010, United States

[§]Departamento de Química Orgánica, Universidad de Granada, Avenida Fuentenueva S/N, 18071 Granada, Spain

Supporting Information

ABSTRACT: The development of protective self-detoxifying materials is an important societal challenge to counteract risk of attacks employing highly toxic chemical warfare agents (CWAs). In this work, we have developed bifunctional zirconium metal–organic frameworks (MOFs) incorporating variable amounts of nucleophilic amino residues by means of formation of the mixed ligand $[Zr_6O_4(OH)_4(bdc)_{6(1-x)}(bdc\text{-}NH_2)_{6x}]$ (**UiO-66-xNH$_2$**) and $[Zr_6O_4(OH)_4(bpdc)_{6(1-x)}(bpdc\text{-}(NH_2)_2)_{6x}]$ (**UiO-67-*x*(NH$_2$)$_2$**) systems where bdc = benzene-1,4-dicarboxylate; bdc-NH$_2$= benzene-2-amino-1,4-dicarboxylate; bpdc = 4,4′-biphenyldicarboxylate; bpdc-(NH$_2$)$_2$ = 2,2′-diamino-4,4′-biphenyldicarboxylate and *x* = 0, 0.25, 0.5, 0.75, 1. In a second step, the **UiO-66-*x*NH$_2$** and **UiO-67-*x*(NH$_2$)$_2$** systems have been postsynthetically modified by introduction of highly basic lithium tert-butoxide (Li^{t}Bu) on the oxohydroxometallic clusters of the mixed ligand MOFs to yield **UiO-66-*x*NH$_2$@LiO^{t}Bu** and **UiO-67-*x*(NH$_2$)$_2$@LiO^{t}Bu** materials. The results show that the combination of pre and postsynthetic modifications on these MOF series gives rise to fine-tuning of the catalytic activity toward the hydrolytic degradation of both simulants and real CWAs in unbuffered aqueous solutions. Indeed, **UiO-66-0.25NH$_2$@LiO^{t}Bu** is able to hydrolyze both CWAs simulants (diisopropylfluorophosphate (DIFP), 2-chloroethylethylsulfide (CEES), and real CWAs (soman (GD), sulfur mustard (HD)) quickly in aqueous solution. These results are related to a suitable combination of robustness, nucleophilicity, basicity, and accessibility to the porous framework.

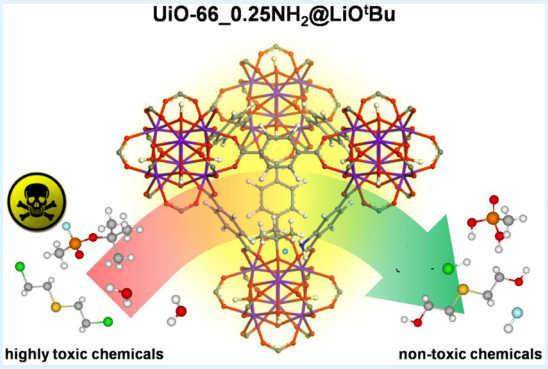

KEYWORDS: *nerve agents, catalysis, hydrolysis, toxic gases, degradation, adsorption, porous coordination frameworks, phosphotriesterase*

INTRODUCTION

Chemical warfare agents (CWAs) are highly toxic chemical compounds that represent an extreme risk to society[1] with the peril of terrorist attacks and conflicts such as in Syria, where stockpiles were discovered and the United Nations believes sarin (GB) was used.[2] As a consequence of this threat, there is an urgent need for the development of materials for protection, detection, and decontamination of CWAs. The development of more efficient materials for protection toward CWAs is a growing research area and has attracted a great deal of interest from the scientific community in the past few years.[3] Current state-of-the-art protective materials consist of activated carbon[4] supplemented with metal nanoparticles and/or organic amines,[5] however, they suffer from deactivation problems. Other alternative approaches consisting of catalytically active metal oxides have also been explored, however, they are limited in terms of low adsorption capacity and/or low range of activity.[6,7] There is consequently a need for a new generation of advanced self-detoxifying materials capable of adsorbing and degrading a broad range of toxic agents in actual application conditions (i.e., ambient temperature and humidity). In this regard, we can take advantage of the designable flexibility of metal–organic frameworks (MOFs), a highly versatile class of porous materials, constituted by metal ions/clusters (or Secundary Building Units, SBUs) connected by organic spacers, that give rise to extended porous networks. MOFs are among the most porous materials known to date, (with porous surfaces up to 7000 m^2g^{-1}) offering the possibility of precise tuning of

Received: May 5, 2017
Accepted: June 27, 2017
Published: June 27, 2017

DOI: 10.1021/acsami.7b06341
ACS Appl. Mater. Interfaces 2017, 9, 23967–23973

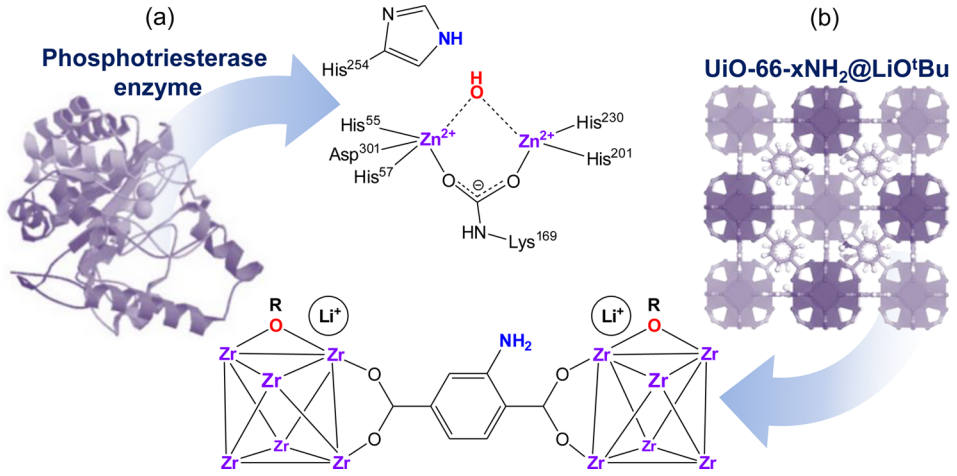

Figure 1. Comparison between active sites of (a) phosphotriesterase enzyme and (b) bifunctionalized UiO-66-xNH$_2$@LiO^{t}Bu materials prepared in this work, containing Lewis acidic sites (magenta), basic sites (red), and amino-nucleophilic sites (blue).

their adsorption and catalytic sites.[8,9] All these features make them ideal platforms for capture, sensing and decontamination of CWAs.[10−14] Among them, Zirconium-based MOFs, and particularly the prototypical UiO-66 [$Zr_6O_4(OH)_4(bdc)_6$] system, characterized by its robustness,[15−18] show promising catalytic activity for the hydrolytic degradation of phosphate ester bonds found in nerve agents. This has been related to a suitable combination of Lewis acidity and basicity of zirconium and hydroxide groups, respectively, resembling in some aspects the phosphotriesterase enzyme active center (Figure 1).[19] However, these systems are prone to deactivation as a consequence of irreversible binding of the nerve agent degradation products to the oxohydroxometal cluster,[20,21] being beneficial for the use of basic species to regenerate the catalytically active sites.[15]

The incorporation of nucleophilic sites in the structure of MOFs has proven beneficial for the degradation of nerve agent simulants. Thus, the functionalization of NH$_2$-MIL-101 (Al) and NH$_2$-MIL-53 (Al) systems, which are catalytically inactive, with nucleophilic 4-methylaminopyridine (4-MAP) residues gives rise to high catalytically active materials for the degradation of P−F bonds of the nerve agent simulant diisopropylfluorophosphate (DIFP).[22] On a different approach Farha et al. studied the effect of the introduction of NH$_2$ groups on [$Zr_6O_4(OH)_4$(bdc-NH$_2$)$_6$] (**UiO-66-NH$_2$**) and [$Zr_6O_4(OH)_4$(bpdc-NH$_2$)$_6$] (**UiO-67-NH$_2$**) systems observing up to 20-fold enhancement of reaction rate compared to pristine UiO-66 and UiO-67 materials in aqueous basic buffered solutions.[23]

Following a different strategy, our group successfully introduced basic sites, acid sites and defects, in the crystalline structure of **UiO-66** via postsynthetic treatment.[21] The results show that the catalytic activity of **UiO-66**, in the hydrolytic degradation of P−F and P−O bonds found in nerve agent simulants, as well as C−Cl bonds found in blister agent simulants, is boosted by the introduction of basic lithium alkoxides in unbuffered aqueous solutions.[21] Likewise, others have also observed that the incorporation of basic species into the porous framework of zirconium MOFs gives rise to the catalytic degradation of nerve agents activity in unbuffered aqueous media.[24]

Taking these precedents into account, we hypothesized that there might be synergistic effects upon simultaneous incorporation of amino nucleophilic groups attached to the organic linker and basic lithium alkoxides in the oxohydroxometallic cluster of zirconium-based MOFs in order to improve their catalytic activity (Figure 1). We further propose that the catalytic activity of the resulting materials might be influenced by four factors: (i) length of the organic spacer and its concomitant effect on framework stability and accessibility; (ii) the bulk of the amino residues and the associated accessibility to the porous structure; (iii) the concentration of nucleophilic amino residues on the MOF pore surface; and (iv) the enhanced basicity of zirconium metal cluster after LiO^{t}Bu incorporation.

RESULTS AND DISCUSSION

Taking into account all of the above considerations, we have prepared the MOFs [$Zr_6O_4(OH)_4$(bdc)$_{6(1-x)}$(bdc-NH$_2$)$_{6x}$] (**UiO-66-xNH$_2$**) and [$Zr_6O_4(OH)_4$(bpdc)$_{6(1-x)}$ (bpdc-(NH$_2$)$_2$)$_{6x}$] (**UiO-67-x(NH$_2$)$_2$**) (where x = 0, 0.25, 0.5, 0.75, 1) by reaction of $ZrCl_4$ with an appropriate mixture of the organic linkers (Figure 2 and the Supporting Information, SI). In a second step, the as-synthesized mixed ligand MOFs were modified postsynthetically by the introduction of LiO^{t}Bu basic sites, following the procedure of Long et al.,[25] in order to give rise to bifunctionalized materials of [$Zr_6O_4(OH)_4$(bdc)$_{6(1-x)}$(bdc-NH$_2$)$_{6x}$]·(LiO^{t}Bu)$_{0.33}$ (**UiO-66-xNH$_2$@LiO^{t}Bu**) and [$Zr_6O_4(OH)_4$(bpdc)$_{6(1-x)}$(bpdc-(NH$_2$)$_2$)$_{6x}$]·(LiO^{t}Bu)$_{0.33}$ (**UiO-67-x(NH$_2$)$_2$@LiO^{t}Bu**) type.

The composition and phase purity of the **UiO-66-xNH$_2$** and **UiO-67-x(NH$_2$)$_2$** mixed ligand MOFs was assessed by means of TGA, CHN elemental analysis, and X-ray powder diffraction (Figures S1−S4 and SI). ^{1}H NMR of hydrolyzed materials was used to determine the aminated spacer present in the materials. The results show the formation of defective **UiO-66-xNH$_2$** and **UiO-67-x(NH$_2$)$_2$** materials with the SBU connectivity varying from 6.5 in **UiO-66-NH$_2$** to 11 in **UiO-67-0.5(NH$_2$)$_2$**. These results are in agreement with previously reported works suggesting the formation of defective **fcu** networks which is facilitated by the use of coordination modulators.[26,27] The N$_2$ adsorption (77 K) results agree with the porous nature of these systems, although, as expected, the accessibility to the porous structure is diminished by the bulk of the amino residues (Figures S6 and S7). Indeed, we have noticed that the adsorption capacity and specific surface area decreases with

DOI: 10.1021/acsami.7b06341
ACS Appl. Mater. Interfaces 2017, 9, 23967−23973

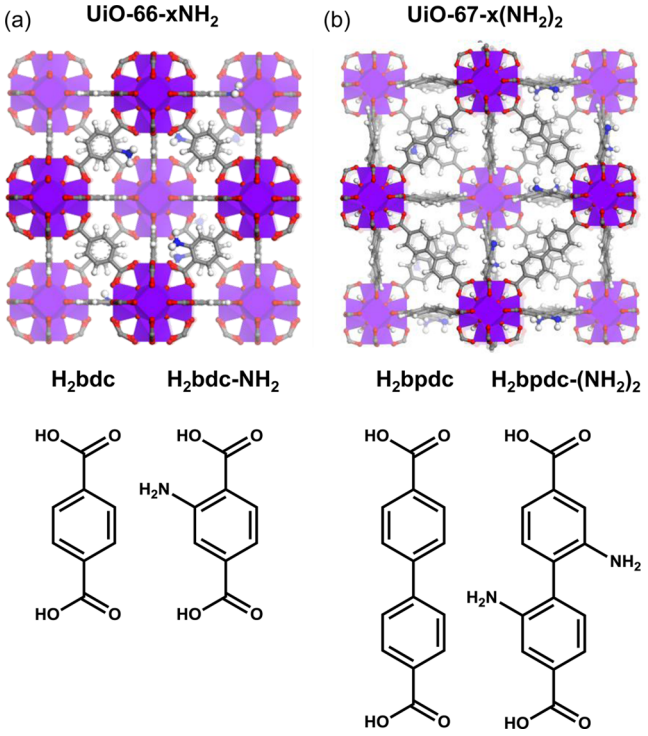

Figure 2. Mixed ligand zirconium based metal−organic framework prepared in this work: (a) $[Zr_6O_4(OH)_4(bdc)_{6(1-x)}(bdc\text{-}NH_2)_{6x}]$ (UiO-66-xNH$_2$) and (b) $[Zr_6O_4(OH)_4(bpdc)_{6(1-x)}(bpdc\text{-}(NH_2)_2)_{6x}]$ (UiO-67-x(NH$_2$)$_2$) with x = 0, 0.25, 0.5, 0.75, 1.

increasing amounts of amino groups in the MOFs. It is noteworthy that while the accessibility to the porous network in the **UiO-66-*x*NH$_2$** series is not highly affected, the end members of **UiO-67-*x*(NH$_2$)$_2$** series exhibit a limited pore accessibility as a probable consequence of the higher density of amino residues. These results are in agreement with literature reports on UiO-66 and UiO-67 derivatized systems in which the specific surface area are significantly reduced by functionalization with one and two amino residues.[28−30]

The postsynthetic treatment of the above prepared MOFs with Li^{t}Bu, following the procedure of Long and co-workers for **UiO-66**,[25] lead to the formation of $[Zr_6O_4(OH)_4(bdc)_{6(1-x)}(bdc\text{-}NH_2)_{6x}](LiO^tBu)_{0.33}$ (**UiO-66-*x*NH$_2$@LiO^{t}Bu**) and $[Zr_6O_4(OH)_4(bpdc)_{6(1-x)}(bpdc\text{-}(NH_2)_2)_{6x}](LiO^tBu)_{0.33}$ (**UiO-67-*x*(NH$_2$)$_2$@LiO^{t}Bu**) composite materials. The postsynthetically modified materials are crystalline, however, the treatment of Li^{t}Bu is responsible for a decrease of materials crystallinity and surface area which is in agreement with previous results on Ui-O66@Li^{t}Bu.[21,25] Moreover, the end members of the UiO-67-x(NH$_2$)$_2$@Li^{t}Bu series exhibit a significant decrease of material crystallinity and low N_2 adsorption capacities indicative of partial collapse of the porous structure (Figures S4b, S5b, S6b, S7b). The latter results are in agreement with previous findings of diminished stability of zirconium frameworks containing amino functionalized organic linkers.[18]

Once the prepared materials were characterized, we proceeded to study the impact of both the presence of nucleophilic amino residues and the basic lithium alkoxides on their catalytic activity. The materials were tested on the hydrolytic degradation of DIFP and CEES using a cluster-simulant 1:1 stoichiometric ratio, in unbuffered aqueous solutions, in order to reproduce real operational conditions as laid out in detail in the SI. The profiles and kinetic constants for hydrolytic degradation of DIFP by **UiO-66-*x*NH$_2$**, **UiO-67-*x*(NH$_2$)$_2$**, **UiO-66-*x*NH$_2$@LiO^{t}Bu** and **UiO-67-*x*(NH$_2$)$_2$@LiO^{t}Bu** materials are summarized in Figures 3, 4, and 5.

The results for the hydrolytic degradation of DIFP upon contact with the mixed ligand MOFs are indicative that the behavior of the **UiO-66-*x*NH$_2$** amino doped systems is significantly different to pristine **UiO-66** (Figure 3b). Indeed, while **UiO-66** exhibits a rather fast initial degradation speed of DIFP ($t_{1/2}$= 15 min), the catalytic activity dies after aproximately 200 min with 75% degradation of the nerve gas simulant due to catalyst poisoning.[21] By contrast, the **UiO-66-0.25NH$_2$** exhibits an initial lower reaction rate ($t_{1/2}$= 173 min), but an overall higher conversion of 100% after 24 h. The rest of the amino doped systems have a similar behavior with the **UiO-66-0.5NH$_2$** exhibiting the highest rate ($t_{1/2}$ = 41 min) indicative of an optimal balance between framework accesibility and nucleophilicity of the material (Table S1). In order to have a clear idea of the possible mecanism of the catalytic reaction, we have also studied the effect of the addition of equimolecular amounts of methylphosphonic acid (Figure S8a), which is the prototypical degradation product of nerve agents. The results show that the catalytic activity is negatively affected in all cases, although the impact on **UiO-66-0.25NH$_2$** is less pronounced. The inhibition effect of nerve agent degradation products is related to the irreversible coordination to the zirconium metal clusters, as recently stated by Frenkel et al.[20] thereby blocking the catalytically active sites. By contrast, the nerve agent degradation products should not affect the nucleophilic amino residues explaining the overall better performance of the **UiO-66-0.25NH$_2$** system in comparison to pristine **UiO-66**.[21] **UiO-66-1NH$_2$** also exhibits a steady increase of DIFP degradation compared to **UiO-66**, although its activity is below **UiO-66-0.25NH$_2$** as a probable consequence of a limited porous matrix accesibility related to the bulk of amino residues, that should hamper the difussion of DIFP into the active sites of the porous framework. Similar results are observed in the **UiO-67-*x*(NH$_2$)$_2$** series, in which the **UiO-67-0.25(NH$_2$)$_2$** systems exhibit the best performance (Figure 3c).

A significant increase in the catalytic activity is observed after the incorporation of Li^{t}Bu in the **UiO-66-*x*NH$_2$@LiO^{t}Bu** materials. Thus, **UiO-66-0.25NH$_2$@LiO^{t}Bu** exhibits the fastest reaction rate, with a $t_{1/2}$ of 0.4 min (Figures 3b, 4a, and 5). This is a significant improvement with regard to both pristine **UiO-66** and **UiO-66@LiO^{t}Bu** exhibiting $t_{1/2}$ values of 17 and 9.7 min, respectively. Moreover, **UiO-66-0.25NH$_2$@LiO^{t}Bu** maintains its catalytic activity after three cycles (Figure S10). Moreover, we are not able to detect any leaching of Li^{t}Bu (^{1}H NMR) which is indicative that **UiO-66-0.25NH$_2$@LiO^{t}Bu** is solely responsible for the catalytic activity since any possible Li^{t}Bu leached to the supernatant solution should give a lower degradation activity (see Figure S12). Noteworthy, a significant decrease of catalytic activity is observed in the end members of the **UiO-66-*x*NH$_2$@LiO^{t}Bu** series, namely **UiO-66-0.75NH$_2$@LiO^{t}Bu** and **UiO-66-1NH$_2$@LiO^{t}Bu**, which might be related to both crowding of amino groups in the pores and to the lower stability of amino functionalized systems under basic conditions (partial collapse of the framework can be deduced from PXRD and N_2 adsorption data in Figures S4b and S6b). It can be concluded that the doping of amino groups, up to a 0.5 value, by means of the formation of mixed ligand MOFs, gives rise to an adequate balance of accesibility to active sites and framework stability. A closely related trend is also found for the **UiO-67-**

DOI: 10.1021/acsami.7b06341
ACS Appl. Mater. Interfaces 2017, 9, 23967−23973

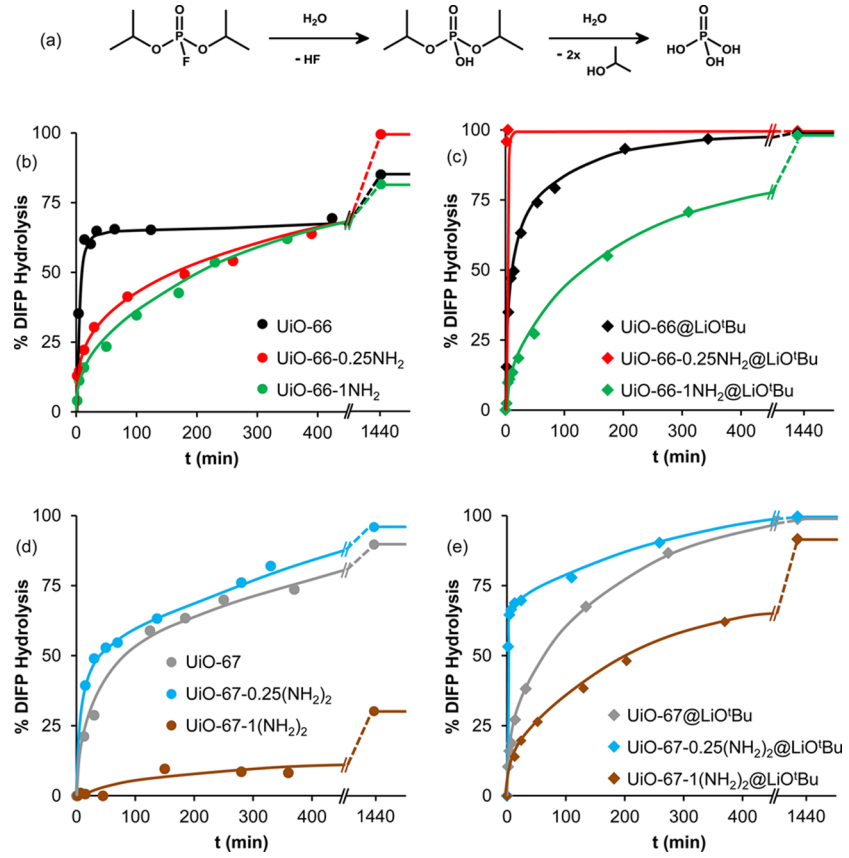

Figure 3. Hydrolytic degradation reaction of DIFP nerve agent simulant (a). Profiles of catalytic hydrolytic degradation of DIFP upon exposure to UiO-66-xNH$_2$ (b), UiO-66-xNH$_2$@LiO^{t}Bu (c), UiO-67-x(NH$_2$)$_2$ (d), and UiO-67-x(NH$_2$)$_2$@LiO^{t}Bu (e) materials (x = 0, 0.25, 1), in aqueous media, at room temperature. The solid lines are a guide to eyes. The catalytic profiles of the complete series are shown in Figures S7 and S8.

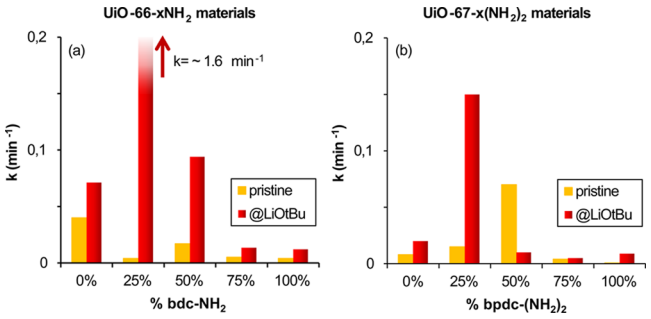

Figure 4. Summary of DIFP hydrolysis reaction rate constant (k) values for (a) UiO-66-xNH$_2$ (yellow) and UiO-66-xNH$_2$@LiO^{t}Bu (red) and for (b) UiO-67-x(NH$_2$)$_2$ (yellow) and UiO-67-x(NH$_2$)$_2$@LiO^{t}Bu (red) materials after fitting the data to a first order kinetic model. Note: Reaction rate constant values of [UiO-66-0.25NH$_2$@LiO^{t}Bu] could not be precisely calculated because of almost instantaneous degradation of DIFP (0% DIFP after 3 min).

x(NH$_2$)$_2$@LiO^{t}Bu material series (Figure 3d and Table S1). Indeed, similarly, **UiO-67-0.25(NH$_2$)$_2$@LiO^{t}Bu** shows the fastest DIFP degradation rate indicative of a synergistic effect between the basic LiO^{t}Bu sites and the amino-nucleophilic sites. Nevertheless, the overall performance of the **UiO-67-x(NH$_2$)$_2$** and **UiO-67-x(NH$_2$)$_2$@LiO^{t}Bu** materials is poorer than their **UiO-66-xNH$_2$@LiO^{t}Bu** counterparts which might be related to the lower hydrolytic stability of **UiO-67** vs **UiO-66**.[18]

In order to further study the reactivity improvement upon incorporation of basic **LiO^{t}Bu** residues, we have studied the possible poisoning of the catalyst by the addition of equimolecular amounts of methylphosphonic acid, phosphoric acid, and fluoride ions to the reaction media (Figure 5). These products can, in principle, be responsible for an acidification of the reaction media and/or coordination to the MOF active sites[20] thereby slowing down the hydrolysis rate (Table S3). The results show that the DIFP degradation profiles exhibit a small effect upon addition of the typical nerve agent degradation products for **UiO-66-0.25NH$_2$@LiO^{t}Bu** and slightly higher for **UiO-67-0.25(NH$_2$)$_2$@LiO^{t}Bu**.

These results represent a clear improvement in comparison with pristine **UiO-66-xNH$_2$** systems (Figure S8a) being indicative of the ability of LiO^{t}Bu to prevent the poisoning of the MOF active sites as previously shown by us for **UiO-66@LiO^{t}Bu**.[21]

In order to further prove the catalytic performance of our materials we have also evaluated the behavior of our systems toward the degradation of vesicant agents using 2-chloroethylethylsulfide (CEES) as model of sulfur mustard (HD). In this regard, it should be noted that while zirconium MOFs are highly active in the degradation of P−X bonds (X = F, Cl, S, O) typically found in nerve agents they are poorly active in the hydrolytic degradation of C−Cl of vesicant agents.[13] This represents a limitation for the practical application of these systems in which the chemical threat is unknown. In this regard, we have found that the incorporation of amino residues and basic LiO^{t}Bu leads to a synergistic effect for the degradation of C−Cl bonds found in simulant CEES which can be taken as prove of the multifunctional protective nature

DOI: 10.1021/acsami.7b06341
ACS Appl. Mater. Interfaces 2017, 9, 23967−23973

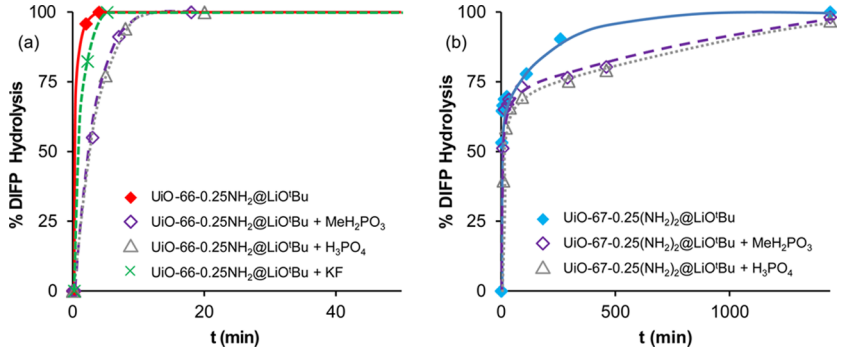

Figure 5. Profiles of catalytic hydrolytic degradation of DIFP upon exposure to the (a) UiO-66-0.25NH_2@LiO^tBu and (b) UiO-67-0.25$(NH_2)_2$@LiO^tBu materials, in the presence of equimolecular amounts of methylphosphonic acid, potasium fluoride and phosphoric acid.

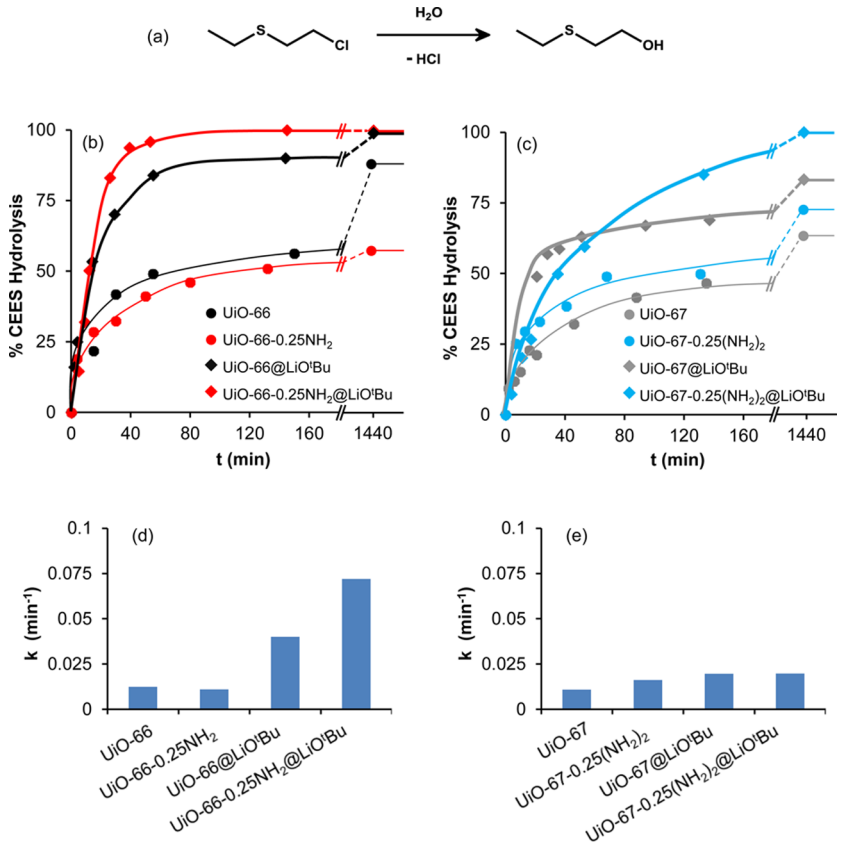

Figure 6. (a) Hydrolytic degradation reaction of the sulfur mustard simulant CEES. Profiles and kinetic k constants (min^{-1}) for catalytic hydrolytic degradation of CEES upon exposure to the (b,d) UiO-66-$x$$NH_2$, and UiO-66-$x$$NH_2$@Li$O^t$Bu; (c,e) UiO-67-$x$$(NH_2)_2$ and UiO-67-$x$$(NH_2)_2$@Li$O^t$Bu ($x$ = 0, 0.25, 1) materials, in aqueous-ethanolic media, at room temperature.

of these materials (Figure 6). Indeed, **UiO-66-0.25NH_2@LiO^tBu** exhibits the fastest reaction rate, with a 9.6 min $t_{1/2}$ value in the degradation of CEES. This represent a significant improvement in comparison to both pristine **UiO-66** and **UiO-66@LiO^tBu** exhibiting $t_{1/2}$ values of 56 and 17.3 min, respectively (Table S2). Similar results are observed for **UiO-67-$x$$(NH_2)_2$** series, where **UiO-67-0.25$(NH_2)_2$@LiO^tBu** shows the best catalytic performance, achieving full conversion of CEES, after 24 h.

Finally, in order to prove the practical utility of the synergistic combination of basic and nucleophilic sites on zirconium MOFs in the degradation of real CWAs, we have evaluated the catalytic activity of **UiO-66**, **UiO-66@LiO^tBu**, and **UiO-66-0.25NH_2@LiO^tBu** materials toward the hydrolytic degradation of real CWAs, namely the nerve agent Soman (GD) and the vesicant agent sulfur mustard (HD) (Figure 7). As with DIFP and CEES simulants, the introduction of LiO^tBu and amino groups leads to a synergistic effect for the hydrolytic degradation of both the P−F and C−Cl bonds of soman and sulfur mustard, respectively. It should be noted that hydrolysis of soman by **UiO-66@LiO^tBu** and **UiO-66-0.25NH_2@LiO^tBu** materials are both instantaneous. In the case of sulfur mustard, the results clearly point to a synergistic effect of the introduction of basic LiO^tBu and nucleophilic amino residues in **UiO-66-0.25NH_2@LiO^tBu** material for C−Cl bond breaking with a 19 min $t_{1/2}$ value in the degradation of HD.

DOI: 10.1021/acsami.7b06341
ACS Appl. Mater. Interfaces 2017, 9, 23967−23973

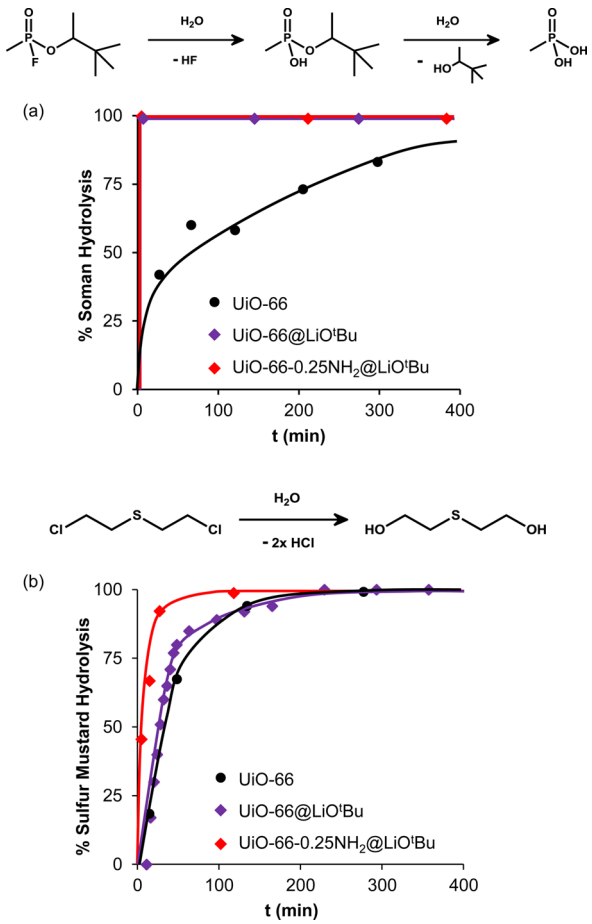

Figure 7. Profiles of catalytic hydrolytic degradation of real CWAs: (a) soman gas and (b) mustard gas CWAs upon exposure to UiO-66, UiO-66@LiO^{t}Bu and UiO-66-0.25NH_2@LiO^{t}Bu materials.

CONCLUSIONS

We show that the doping of archetypical zirconium MOF frameworks with nucleophilic amino and basic lithium alkoxides gives rise to a synergistic effect leading to bifunctional catalytic activity for the hydrolytic degradation of both C−Cl bonds of vesicant mustard gas as well as P−F bond of soman nerve agent. This behavior is a consequence of the optimal balance between framework stability, nucleophilicity, basicity, and accessibility to the catalytic active sites. This work also demonstrates that the formation of mixed ligand MOFs paves the way for fine-tuning of the adsorptive and catalytic properties of MOFs for specific applications.

ASSOCIATED CONTENT

Supporting Information

The Supporting Information is available free of charge on the ACS Publications website at DOI: 10.1021/acsami.7b06341.

Details of materials, methods, synthesis, physicochemical characterization, and catalytic degradation of real and simulant CWAs (PDF)

AUTHOR INFORMATION

Corresponding Author

*E-mail: jarn@ugr.es (J.A.R.N.).

ORCID

Gregory W. Peterson: 0000-0003-3467-5295

Jared B. DeCoste: 0000-0003-0345-2697

L. Marleny Rodríguez-Albelo: 0000-0001-6172-1918

Elisa Barea: 0000-0001-9895-1047

Jorge A. R. Navarro: 0000-0002-8359-0397

Notes

The authors declare no competing financial interest.

ACKNOWLEDGMENTS

The authors are grateful to generous funding from Spanish MINECO (CTQ2014-53486-R; CTQ2015-70724-R), EU Feder funding, and the Joint Science and Technology Office for Chemical Biological Defense (JSTO−CBD) under project BA13PHM210.

REFERENCES

(1) https://www.opcw.org/; accessed June 27, 2017.

(2) United Nations Mission to Investigate Allegations of the Use of Chemical Weapons in the Syrian Arab Republic. http://undocs.org/A/68/663; accessed June 27, 2017.

(3) Szinicz, L. History of chemical and biological warfare agents. *Toxicology* **2005**, *214*, 167−181.

(4) *Self-Cleaning Materials and Surfaces*; John Wiley & Sons Ltd.: New York, 2013.

(5) Smith, J. W. H.; Romero, J. V.; Dahn, T. R.; Dunphy, K.; Croll, L. M.; Dahn, J. R. Effect of co-impregnated acids on performance of Zn-based broad spectrum respirator carbons. *J. Hazard. Mater.* **2012**, *235*, 279−285.

(6) Bandosz, T. J.; Laskoski, M.; Mahle, J.; Mogilevsky, G.; Peterson, G. W.; Rossin, J. A.; Wagner, G. W. Reactions of VX, GD, and HD with Zr(OH)4: Near Instantaneous Decontamination of VX. *J. Phys. Chem. C* **2012**, *116*, 11606−11614.

(7) Kim, S.; Ying, W. B.; Jung, H.; Ryu, S. G.; Lee, B.; Lee, K. J. Zirconium Hydroxide-coated Nanofiber Mats for Nerve Agent Decontamination. *Chem. - Asian J.* **2017**, *12*, 698.

(8) Furukawa, H.; Cordova, K. E.; O'Keeffe, M.; Yaghi, O. M. The chemistry and applications of metal-organic frameworks. *Science* **2013**, *341*, 1230444.

(9) Slater, A. G.; Cooper, A. I. Function-led design of new porous materials. *Science* **2015**, *348*, 6238.

(10) Bobbitt, N. S.; Mendonca, M. L.; Howarth, A. J.; Islamoglu, T.; Hupp, J. T.; Farha, O. K.; Snurr, R. Q. Metal−organic frameworks for the removal of toxic industrial chemicals and chemical warfare agents. *Chem. Soc. Rev.* **2017**, *46*, 3357.

(11) DeCoste, J. B.; Peterson, G. W. Metal-organic frameworks for air purification of toxic chemicals. *Chem. Rev.* **2014**, *114*, 5695−5727.

(12) Barea, E.; Montoro, C.; Navarro, J. A. R. Toxic gas removal - Metal organic frameworks for the capture and degradation of toxic gases and vapours. *Chem. Soc. Rev.* **2014**, *43*, 5419−5430.

(13) Liu, Y.; Howarth, A. J.; Vermeulen, N. A.; Moon, S.-Y.; Hupp, J. T.; Farha, O. K. *Coord. Chem. Rev.* **2017**, *346*, 101−111.

(14) Stassen, I.; Bueken, B.; Reinsch, H.; Oudenhoven, J. F. M.; Wouters, D.; Hajek, J.; Van Speybroeck, V.; Stock, N.; Vereecken, P. M.; Van Schaijk, R.; De Vos, D.; Ameloot, R. Towards metal-organic framework based field effect chemical sensors: UiO-66-NH2 for nerve agent detection. *Chem. Sci.* **2016**, *7*, 5827−5832.

(15) Mondloch, J. E.; Katz, M. J.; Isley, W. C., III; Ghosh, P.; Liao, P.; Bury, W.; Wagner, G. W.; Hall, M. G.; DeCoste, J. B.; Peterson, G. W.; Snurr, R. Q.; Cramer, C. J.; Hupp, J. T.; Farha, O. K. Destruction of chemical warfare agents using metal−organic frameworks. *Nat. Mater.* **2015**, *14*, 512−516.

(16) Cavka, J. H.; Jakobsen, S.; Olsbye, U.; Guillou, N.; Lamberti, C.; Bordiga, S.; Lillerud, K. P. A new zirconium inorganic building brick forming metal organic frameworks with exceptional stability. *J. Am. Chem. Soc.* **2008**, *130*, 13850−13851.

(17) Bai, Y.; Dou, Y.; Xie, L.-H.; Rutledge, W.; Li, J.-R.; Zhou, H.-C. Zr-based metal-organic frameworks: design, synthesis, structure, and applications. *Chem. Soc. Rev.* **2016**, *45*, 2327−2367.

DOI: 10.1021/acsami.7b06341
ACS Appl. Mater. Interfaces 2017, 9, 23967−23973

(18) DeCoste, J. B.; Peterson, G. W.; Jasuja, H.; Glover, T. G.; Huang, Y.; Walton, K. S. Stability and degradation mechanisms of metal−organic frameworks containing the Zr6O4(OH)4 secondary building unit. *J. Mater. Chem. A* **2013**, *1*, 5642−5650.
(19) Katz, M. J.; Mondloch, J. E.; Totten, R. K.; Park, J. K.; Nguyen, S. T.; Farha, O. K.; Hupp, J. T. Simple and Compelling Biomimetic Metal−Organic Framework Catalyst for the Degradation of Nerve Agent Simulant. *Angew. Chem., Int. Ed.* **2014**, *53*, 497−501.
(20) Plonka, A. M.; Wang, Q.; Gordon, W. O.; Balboa, A.; Troya, D.; Guo, W.; Sharp, C. H.; Senanayake, S. D.; Morris, J. R.; Hill, C. L.; Frenkel, A. I. In Situ Probes of Capture and Decomposition of Chemical Warfare Agent Simulants by Zr-Based Metal Organic Frameworks. *J. Am. Chem. Soc.* **2017**, *139* (2), 599−602.
(21) López-Maya, E.; Montoro, C.; Rodríguez-Albelo, L. M.; Aznar Cervantes, S. D.; Lozano-Pérez, A. A.; Cenís, J. L.; Barea, E.; Navarro, J. A. R. Textile-metal-organic framework composites as self-detoxifying filters for chemical warfare agents. *Angew. Chem., Int. Ed.* **2015**, *54*, 6790−6794.
(22) Bromberg, L.; Klichko, Y.; Chang, E. P.; Speakman, S.; Straut, C. M.; Wilusz, E.; Hatton, T. A. Alkylaminopyridine-modified aluminum aminoterephthalate metal-organic frameworks as components of reactive self-detoxifying materials. *ACS Appl. Mater. Interfaces* **2012**, *4*, 4595−4602.
(23) Katz, M. J.; Moon, S.-Y.; Mondloch, J. E.; Beyzavi, M. H.; Stephenson, C. J.; Hupp, J. T.; Farha, O. K. Exploiting parameter space in MOFs: a 20-fold enhancement of phosphate-ester hydrolysis with UiO-66-NH2. *Chem. Sci.* **2015**, *6*, 2286−2291.
(24) Moon, S.-Y.; Proussaloglou, E.; Peterson, G. W.; DeCoste, J. B.; Hall, M. G.; Howarth, A. J.; Hupp, J. T.; Farha, O. K. Detoxification of Chemical Warfare Agents Using a Zr6 -Based Metal-Organic Framework/Polymer Mixture. *Chem. - Eur. J.* **2016**, *22*, 14864−14868.
(25) Ameloot, R.; Aubrey, M.; Wiers, B. M.; Gomora-Figueroa, A. P.; Patel, S. N.; Balsara, N. P.; Long, J. R. Ionic Conductivity in the Metal−Organic Framework UiO-66 by Dehydration and Insertion of Lithium tert-Butoxide. *Chem. - Eur. J.* **2013**, *19*, 5533−5536.
(26) DeStefano, M. R.; Islamoglu, T.; Garibay, S. J.; Hupp, J. T.; Farha, O. K. Room-Temperature Synthesis of UiO-66 and Thermal Modulation of Densities of Defect Sites. *Chem. Mater.* **2017**, *29*, 1357−1361.
(27) Vermoortele, F.; Bueken, B.; Le Bars, G.; Van de Voorde, B.; Vandichel, M.; Houthoofd, K.; Kirschhock, C. Synthesis modulation as a tool to increase the catalytic activity of metal−organic frameworks: the unique case of UiO-66 (Zr). *J. Am. Chem. Soc.* **2013**, *135*, 11465−11468.
(28) Katz, M. J.; Brown, Z. J.; Colón, Y. J.; Siu, P. W.; Scheidt, K. A.; Snurr, R. Q.; Hupp, J. T.; Farha, O. K. A facile synthesis of UiO-66, UiO-67 and their derivatives. *Chem. Commun.* **2013**, *49*, 9449−9451.
(29) Biswas, S.; Van Der Voort, P. A General Strategy for the Synthesis of Functionalised UiO-66 Frameworks: Characterisation, Stability and CO2 Adsorption Properties. *Eur. J. Inorg. Chem.* **2013**, *2013*, 2154−2160.
(30) Ko, N.; Hong, J.; Sung, S.; Cordova, K. E.; Park, H. J.; Yang, J. K.; Kim, J. A significant enhancement of water vapour uptake at low pressure by amine-functionalization of UiO-67. *Dalton Trans.* **2015**, *44*, 2047−2051.

DOI: 10.1021/acsami.7b06341
ACS Appl. Mater. Interfaces 2017, 9, 23967−23973